Effect of Rds abundance on cone outer segment morphogenesis, photoreceptor gene expression, and outer limiting membrane integrity

ARTICLE *in* THE JOURNAL OF COMPARATIVE NEUROLOGY · OCTOBER 2007

Impact Factor: 3.23 · DOI: 10.1002/cne.21476 · Source: PubMed

3 AUTHORS, INCLUDING:

Steven Fliesler
University at Buffalo, The State University of …

135 PUBLICATIONS **3,421** CITATIONS

SEE PROFILE

Published in final edited form as:
J Comp Neurol. 2007 October 20; 504(6): 619–630.

Effect of Rds Abundance on Cone Outer Segment Morphogenesis, Photoreceptor Gene Expression, and Outer Limiting Membrane Integrity

RAFAL FARJO[1], **STEVEN J. FLIESLER**[2], and **MUNA I. NAASH**[1,*]

1 *Department of Cell Biology, University of Oklahoma Health Sciences Center, Oklahoma City, Oklahoma 73104*

2 *Departments of Ophthalmology and Pharmacological and Physiological Science, St. Louis University School of Medicine, St. Louis, Missouri 63104*

Abstract

We examined the molecular, structural, and functional consequences on cone photoreceptors of the neural retinal leucine zipper knockout ($Nrl^{-/-}$) mice when only one allele of retinal degeneration slow (Rds) is present ($Rds^{+/-}/Nrl^{-/-}$). Quantitative RT-PCR and immunoblot analysis were used to assess the expression levels of several phototransduction genes; electroretinography was used to assess quantitatively the retinal responsiveness to light; and immunohistochemistry and ultrastructural analysis were used to examine retinal protein distribution and morphology, respectively. In Rds/Nrl double-null mice, S-cones form dysmorphic outer segments that lack lamellae and fail to associate properly with the cone matrix sheath and the outer limiting membrane. In $Rds^{+/-}/Nrl^{-/-}$ mice, cones form oversized and disorganized outer segment lamellae; although outer limiting membrane associations are maintained, normal interactions with cone matrix sheaths are not, and photoreceptor rosette formation is observed. These retinas produce significantly higher photopic a-wave and b-wave amplitudes than do those of $Rds^{-/-}/Nrl^{-/-}$ mice, and the levels of several cone phototransduction genes are significantly increased coincidently with the presence of Rds and partial lamellae formation. Thus, as in rod photoreceptors, expression of only one Rds allele is unable to support normal outer segment morphogenesis in cones. However, cone lamellae assembly, albeit disorganized, concomitantly permits outer limiting membrane association, and this appears to be linked to photoreceptor rosette formation in the rodless (cone-only) $Nrl^{-/-}$retina. In addition, photoreceptor gene expression alterations occur in parallel with changes in Rds levels.

Indexing terms

Rds; Nrl; retina; cone photoreceptor; rosette; gene expression

Visual transduction begins when a photon of light is absorbed by a visual pigment chromophore in the outer segment of the photoreceptor cell. In rod photoreceptors, the outer segment consists of stacks of membranous “discs” that are physically separated from the plasma membrane by cytosol; however, in cone photoreceptors, these discs are contiguous with the plasma membrane and are called “lamellae” (Arikawa et al., 1992;Steinberg et al., 1980). Outer segment morphogenesis is an active process. In mammals, nearly 10% of these discs/lamellae are shed by the photoreceptor cells and subsequently phagocytosed by the retinal pigment

*Correspondence to: Muna I. Naash, University of Oklahoma Health Sciences Center, 940 Stanton L. Young Blvd., BMSB 781, Oklahoma City, OK 73104. E-mail: muna-naash@ouhsc.edu

This article includes Supplementary Material available via the Internet at http://www.interscience.wiley.com/jpages/0021-9967/suppmat.

epithelium (RPE) each day, and a comparable amount of new discs/lamellae must be produced and added to maintain the constant length of the outer segment. The proper formation of rod and cone outer segment discs/lamellae is proposed to be governed by a series of evagination and invagination events that are reliant on the function of the retinal degeneration slow (Rds) protein (Boesze-Battaglia and Goldberg, 2002;Damek-Poprawa et al., 2005;Eckmiller, 1987, 1990;Farjo et al., 2006;Goldberg, 2006;Ritter et al., 2004;Steinberg et al., 1980).

In rod photoreceptors, the absence of Rds causes aborted disc morphogenesis and a complete absence of outer segment formation (Sanyal and Jansen, 1981), although vesicles containing rhodopsin are present at the tip of the connecting cilium (Nir and Papermaster, 1986). The lack of Rds and resultant absence of outer segment formation cause rod photoreceptors to enter apoptosis, which eventually destroys the entire photoreceptor cell layer (Sanyal and Zeilmaker, 1984). Recently, we demonstrated that the absence of Rds has a different effect on cone photoreceptors (Farjo et al., 2006). Superimposing the $Rds^{-/-}$ mutation on a genetic background where the neural retina leucine zipper gene is knocked out ($Nrl^{-/-}$) results in formation of a retina whose photoreceptor population consists solely of cones and is highly enriched in short-wavelength cones (S-cones; Daniele et al., 2005;Mears et al., 2001;Nikonov et al., 2005;Yoshida et al., 2004;Yu et al., 2004). Such genetic manipulation affords the generation of a loss-of-function model ($Rds^{-/-}/Nrl^{-/-}$) that allows the examination of Rds function specifically in cones (Farjo et al., 2006). In contrast to rods, cones do form outer segment structures in the absence of Rds; however, they lack normal lamellar organization, thus implicating Rds in the process of cone outer segment lamellae formation. These dysmorphic outer segment structures are capable of robust phototransduction.

Previous studies in the rod-dominant wild-type (WT) retina have suggested that one allele of Rds is insufficient to produce well-organized outer segment structures in both rods and cones (Cheng et al., 1997;Hawkins et al., 1985;Jansen et al., 1987;Sanyal et al., 1986); however, these results may be biased by the overwhelming presence of rod photoreceptors. To determine the contribution of a single allele of Rds to cone outer segment morphogenesis, $Rds^{+/-}/Nrl^{-/-}$ mice were generated and characterized in the present study. Herein, we demonstrate that these mice have retinas with increased electrophysiological function when compared with double-null ($Rds^{-/-}/Nrl^{-/-}$) mice, but this level is still lower than that in the $Nrl^{-/-}$mice. Although Rds and its nonglycosylated homologue, rod outer segment membrane-protein 1 (Rom-1), are localized to the outer segment in $Rds^{+/-}/Nrl^{-/-}$ mice, they are unable to make lamellae with normal ultrastructure; instead, highly disorganized and excessively elongated whorls of outer segment membranes are formed. The formation of these disorganized outer segment structures seems to enhance the steady-state level of S-cone opsin and affects the mRNA and/or protein abundance of several other cone phototransduction genes. Furthermore, we demonstrate that the presence of Rds and lamellae formation has secondary effects on the outer limiting membrane (OLM), the network of junctional complexes between photoreceptors and Müller glial cells.

MATERIALS AND METHODS

Animals

All experiments and animal maintenance were approved by the University of Oklahoma's Institutional Animal Care and Use Committee (IACUC) and conformed to the guidelines on the care and use of animals adopted by the Society for Neuroscience and the Association for Research in Vision and Ophthalmology (Rockville, MD). The $Nrl^{-/-}$ mice were kindly provided by Dr. Anand Swaroop (University of Michigan Kellogg Eye Center, Ann Arbor, MI). The $Rds^{-/-}$ mice were kindly provided by Dr. Neeraj Agarwal (University of North Texas Health Science Center, Fort Worth, TX). All mice were bred into and assessed on a C57BL/6 background.

Materials

Commonly employed biochemical reagents, solvents, electrophoresis chemicals, and supplies were used as obtained from various commercial vendors.

Quantitative RT-PCR

Quantitative RT-PCR (qRT-PCR) was performed as previously described (Farjo et al., 2006). Briefly, total RNA was extracted from three pairs of eyes for each genotype at postnatal day 30 (P30) and used for subsequent reverse transcription reactions. qRT-PCR was performed in triplicate on each cDNA sample using an iCycler (Bio-Rad, Hercules, CA), and ΔcT values were calculated against the neuronal "housekeeping" gene hypoxanthine phosphoribosyltransferase (*Hprt*). *Hprt* was assigned an arbitrary expression level of 10,000, and relative gene expression values were calculated with the following equation: Relative expression = $10{,}000/2^{\Delta cT}$, where ΔcT = (*Gene* cT − *Hprt* cT). This was repeated with each of the three total RNA pools isolated for each genotype; expression values are given as the mean with the standard deviation. For examination of glial fibrillary acid protein (*Gfap*) mRNA levels, total RNA was extracted from three pairs of retinas at P21. All primer sequences are available in Supplementary Table 1.

Immunoblotting

Protein extracts were prepared from P30 mouse eyes homogenized on ice and solubilized overnight at 4°C in solubilization buffer (50 mM Tris-HCl, pH 7.5, 100 mM NaCl, 5 mM EDTA, 1% Triton X-100, 0.05% SDS, 2.5% glycerol, and 1.0 mM phenylmethylsulfonyl fluoride). After determination of protein concentrations (micro-BCA method, per the manufacturer's recommended procedures; Pierce, Rockford, IL), 100 μg was loaded on a 10% SDS-PAGE gel and transferred to PVDF membrane for subsequent immunoblotting, essentially as described previously. After blocking with 5% nonfat milk in TBST buffer (25 mM Tris, 140 mM NaCl, 3 mM KCl, 0.05% Tween-20, pH 8.0) for 30 minutes at room temperature (RT), primary antibodies were applied in 5% milk/TBST for 2 hours at RT, followed by three washes in TBST for 10 minutes each. Horseradish peroxidase (HRP)-conjugated secondary antibodies were applied at 1:25,000 dilution in TBST for 50 minutes at RT, followed by four 10-minute washes with TBST. Immunoblot analysis was performed at least three times using biological replicates; in each case, a representative blot is shown. For examination of Gfap protein levels, protein extracts were prepared from retina at P21. For image acquisition and analysis, a Kodak Image Station 440 CF was utilized. Pixel quantification was carried out with Molecular Imaging software (Kodak Inc.).

Immunohistochemistry

Immunohistochemistry was performed on paraffin-embedded ocular sections as previously described (Farjo et al., 2006). Images were acquired with a Hamamatsu C-4742 camera through UPlanSApo objectives (Olympus, Tokyo, Japan) on an Olympus BX62 upright microscope equipped with a spinning disc confocal unit. Projection images were performed with Slidebook v4 software (Olympus). All secondary antibodies (Alexa-488 or Alexa-555 conjugates (Invitrogen, La Jolla, CA) were applied at a dilution of 1:500 from the original stock. For peanut agglutinin staining, Alexa-488-conjugated peanut agglutinin (Invitrogen) was applied at 1:200 dilution during the incubation with secondary antibody.

Antibodies

Primary antibodies, specificity, and dilutions were as follows: rabbit anti-Rds-c-terminal (Rds-cT; polyclonal antibody raised against epitope "QVEAEGADAGPAPEAG" of mouse Rds) antiserum stains monomers and dimers of Rds at ~37 and 74 kD on immunoblot (Ding et al., 2005), 1:1,000; mouse antirhodopsin (1D4; monoclonal antibody raised against epitope

"ETSQVAPA" of bovine rhodopsin, a generous gift from Dr. Robert Molday, University of British Columbia) antiserum stains monomers and dimers of rhodopsin at ~35 and 70 kD on immunoblot (Molday and MacKenzie, 1983), 1:5,000; rabbit anti-S-opsin (polyclonal antibody raised against epitope "MSGEDDFYLFQ" of mouse S-opsin, a generous gift of Dr. Cheryl Craft, University of Southern California) antiserum stains monomers and dimers of S-opsin at ~40 and 80 kD on immunoblot and stains only S-cone outer segments in the retina with immunohistochemistry (Zhu et al., 2003), 1:1,000; rabbit anticone transducin (Gnat2; polyclonal antibody raised against epitope "IDYAEVSCVDNRGQLNNLAD" of bovine cone-transducin and purchased from Santa Cruz Biotechnology, Santa Cruz, CA) antiserum stains a single band of ~40 kD on immunoblot (manufacturer's technical information), 1:1,000; mouse anti-β-actin (monoclonal antibody raised against epitope "DDDIAALVIDNGSGK" of human β-actin and purchased from Sigma-Aldrich, St. Louis, MO) antiserum stains a single band of ~48 kD on immunoblot (manufacturer's technical information), 1:10,000; goat anti-Gfap (polyclonal antibody raised against epitope "KTVEMRDGEVIKESKQEHKDVM" of human Gfap and purchased from Santa Cruz Biotechnology) antiserum stains a single band of ~52kD on immunoblot, 1:1,000; rabbit anti-Rom1 (polyclonal antibody raised against epitope "HKPAPEEAPPDEEPPKE" of mouse Rom1) antiserum stains monomers and dimers of Rom-1 at ~37 and 74 kD on immunoblot (Ding et al., 2005), 1:1,000; and rabbit antiglutamine synthetase (GS; polyclonal antibody raised against epitope "RTCLLNETGDEPFQYKN" of mouse glutamine synthetase and purchased from Sigma-Aldrich) antiserum stains a single band of ~44 kD on immunoblot and stains only Müller glial cells in the adult murine retina (manufacturer's technical information), 1:1,000.

Transmission electron microscopy and plastic-embedment immunogold histochemistry

Transmission electron microscopy and immunogold histochemistry were performed as described in detail previously (Farjo et al., 2006).

Electroretinographic recordings

Electroretinographic (ERG) recordings and analyses were performed as previously described (Farjo et al., 2006). Age-matched WT, $Nrl^{-/-}$, $Rds^{-/-}$, $Rds^{-/-}/Nrl^{-/-}$, and $Rds^{+/-}/Nrl^{-/-}$ mice were examined by photopic (light-adapted) electroretinography at 1, 2, 4, and 12 months of age.

RESULTS

To confirm the generation of $Rds^{+/-}/Nrl^{-/-}$ mice, qRT-PCR (Fig. 1A) and immunoblot analysis (Fig. 1B) were performed to measure respective mRNA and protein levels of Rds at P30. *Rds* mRNA levels were down-regulated by fourfold in $Nrl^{-/-}$ eyes compared with WT eyes, consistent with previously published results (Farjo et al., 2006;Mears et al., 2001;Yoshida et al., 2004;Yu et al., 2004), but were completely absent in $Rds^{-/-}$ and $Rds^{-/-}/Nrl^{-/-}$eyes, as predicted. *Rds* mRNA levels in $Rds^{+/-}/Nrl^{-/-}$ eyes were 49.3% of those in $Nrl^{-/-}$ eyes, and immunoblot densitometry analysis revealed a correlative abundance of Rds protein in the two genotypes. It was also observed that these protein levels were able to produce Rds dimer formation, which is required for the formation of functional Rds complexes necessary for outer segment morphogenesis (Boesze-Battaglia and Goldberg, 2002;Farjo and Naash, 2006;Goldberg, 2006).

The presence of one functional allele of Rds had no impact on the differentiation status of $Rds^{+/-}/Nrl^{-/-}$ retinas. qRT-PCR (Fig. 2A) and immunoblot analysis (Fig. 2B) were performed to measure levels of rhodopsin, which should be absent in the rodless $Nrl^{-/-}$ background. Indeed, rhodopsin mRNA and protein were absent in all eyes from mice with the $Nrl^{-/-}$ genetic background. To confirm further the differentiation status of the $Rds^{+/-}/Nrl^{-/-}$ retina, qRT-PCR

was performed on mouse eyes to quantify the mRNA levels of several rod-specific phototransduction genes (Fig. 2C–F). The mRNAs of the cyclic nucleotide-gated channel alpha-1 (*Cnga1*) and rod transducin (*Gnat1*) were completely abolished in all mice with the $Nrl^{-/-}$ genotype ($P < 0.001$, repeated-measures ANOVA, Bonferroni's multiple-comparisons test). These levels were also greatly reduced in $Rds^{-/-}$ eyes, where the photoreceptor population undergoes degeneration. The mRNA levels of cyclic nucleotide phosphodiesterase 6a (*Pde6a*) and retinal S-antigen (*Sag*) were also decreased by 14-fold and 5-fold, respectively, in the $Nrl^{-/-}$ background, and there was no significant difference in the mRNA abundance of any of these genes between $Rds^{-/-}/Nrl^{-/-}$ and $Rds^{+/-}/Nrl^{-/-}$ eyes ($P > 0.05$, one-way ANOVA, Bonferroni's multiple-comparisons test), indicative that the differentiation status of these cone-like photoreceptors had not been altered by the presence of only one functional Rds allele.

To examine the localization of outer segment-specific proteins, immunohistochemistry was performed on paraffin-embedded ocular sections from P30 $Rds^{-/-}/Nrl^{-/-}$and $Rds^{+/-}/Nrl^{-/-}$ mice. Antibodies against Rds, Rom-1, and S-opsin were utilized to label the outer segment structures (Fig. 3A–F). Rds and Rom-1 were detected by immunostaining in the $Rds^{+/-}/Nrl^{-/-}$ outer segment, but not in the $Rds^{-/-}/Nrl^{-/-}$. This labeling appeared as punctate patches throughout the outer segment layer. Immunostaining of short-wavelength cone opsin (S-opsin) was present in both models; however, outer segment morphology in the $Rds^{+/-}/Nrl^{-/-}$ retina was markedly different from that observed in the $Rds^{-/-}/Nrl^{-/-}$ retina. The outer segment layer of the $Rds^{+/-}/Nrl^{-/-}$ retina also displayed disorganized outer segments; however, punctate patches of staining were evident, possibly indicative of attempted (but abortive) lamellar formation. To determine the precise effect of one allele on cone outer segment morphogenesis, ultrastructural analyses was performed on P30 retinas from $Rds^{+/-}/Nrl^{-/-}$ mice (Fig. 3G). This analysis revealed that the $Rds^{+/-}/Nrl^{-/-}$ outer segment structures comprised disorganized and elongated lamella. These S-cone outer segments formed membranous whorls but appeared to maintain proper contacts with the RPE. Immunogold labeling with anti-S-opsin demonstrated that these outer segment structures contained S-opsin (Fig. 3H). The results are quite similar to those observed in WT rod photoreceptors, where only one copy of Rds is present (Cheng et al., 1997;Jansen et al., 1987).

To assess the affect of Rds presence on photoreceptor function, ERG analysis was performed on WT, $Nrl^{-/-}$, $Rds^{-/-}$, $Rds^{-/-}/Nrl^{-/-}$, and $Rds^{+/-}/Nrl^{-/-}$ mice at multiple time points (Fig. 4). We sought to determine whether expression of only one Rds allele would alter the phototransduction capacity of cone photoreceptors, particularly in comparison with that of the dysmorphic, tubular outer segments observed in photoreceptors in the $Rds^{-/-}/Nrl^{-/-}$retina. Photopic a-wave and b-wave amplitudes were quantified to assess the cone photoreceptor response to light (Fig. 4). As previously observed (Farjo et al., 2006;Mears et al., 2001), the photopic a-wave and b-wave amplitudes of $Nrl^{-/-}$ mice were nearly threefold higher than those of WT mice, because of the replacement of rod photoreceptors with S-cones in the $Nrl^{-/-}$ retina. Although the photopic b-wave amplitude of $Rds^{-/-}/Nrl^{-/-}$ mice also was increased by 25 μV, this was not significantly different from WT eyes ($P > 0.05$, one-way ANOVA, Bonferroni's multiple-comparisons test); however, the mean photopic a-wave amplitudes were increased in the $Rds^{-/-}/Nrl^{-/-}$ by 36 μV, which was significantly different ($P < 0.01$, one-way ANOVA, Bonferroni's multiple-comparisons test). The $Rds^{+/-}/Nrl^{-/-}$ mice displayed photopic a-wave and b-wave amplitudes nearly twofold higher than those of the $Rds^{-/-}/Nrl^{-/-}$ mice, but the mean amplitudes were ~17% less than those observed in the $Nrl^{-/-}$ mice. Upon examination of the photopic ERG time course (Fig. 4B,D), response amplitudes from all genetic backgrounds gradually declined with age and reached nearly identical levels by 12 months of age. The rates of b-wave amplitude decline were nearly linear and comparable in the $Nrl^{-/-}$ and $Rds^{+/-}/Nrl^{-/-}$ mice, being ~41 μV and ~36 μV per month, respectively, throughout the time course examined here. Also, the rates of b-wave amplitude loss in WT and $Rds^{-/-}/Nrl^{-/-}$ mice were comparable to each other, insofar as they declined ~7 μV and ~4 μV per

month, respectively, throughout the time course examined here. We hypothesized, based on these results, that there may be a change in the expression levels of phototransduction genes in the $Rds^{+/-}/Nrl^{-/-}$ to account for these functional differences.

Taken together, the structural analysis and electrophysiology data indicated that cone outer segments with deformed lamellae were better at producing a response to light than having no lamellae at all. We aimed to further assess this phenomenon by examining the levels of key cone phototransduction molecules with qRT-PCR and immunoblot analysis. The mRNA and protein levels of S-opsin in WT, $Nrl^{-/-}$, $Rds^{-/-}$, $Rds^{-/-}/Nrl^{-/-}$, and $Rds^{+/-}/Nrl^{-/-}$ eyes at P30 were initially evaluated (Fig. 5A,B). These analyses revealed that mRNA levels of S-opsin were nearly equal in $Rds^{-/-}/Nrl^{-/-}$ and $Rds^{+/-}/Nrl^{-/-}$ eyes ($P > 0.05$, repeated-measures ANOVA, Bonferroni's multiple-comparisons test); however, 1.84-fold more S-opsin protein was present in the $Rds^{+/-}/Nrl^{-/-}$ eye when examined by immunoblot analysis (Fig. 5C). This level of S-opsin protein in the $Rds^{+/-}/Nrl^{-/-}$ eye was still only ~68% of the total S-opsin protein observed in $Nrl^{-/-}$ retinas. The abundance of Gnat2 mRNA and protein was also examined in these different genetic backgrounds. qRT-PCR analyses of *Gnat2* mRNA levels showed a 2.1-fold increase in $Rds^{+/-}/Nrl^{-/-}$ eyes compared with $Rds^{-/-}/Nrl^{-/-}$ eyes (Fig. 5C). This level of *Gnat2* was also 1.5-fold higher than that observed in $Nrl^{-/-}$ eyes. Densitometric analyses of immunoblots demonstrated that there was 25% more Gnat2 protein in $Rds^{+/-}/Nrl^{-/-}$ eyes than in $Rds^{-/-}/Nrl^{-/-}$ eyes, although both levels were still less than those observed in $Nrl^{-/-}$ eyes (Fig. 5D). These results desmonstrate that altered levels of Rds expression are accompanied by changes in the steady-state levels of other S-cone photoreceptor proteins. Whether these concomitant changes are either a direct or an indirect consequence of changes in Rds abundance per se remains to be determined. To examine this observation further, qRT-PCR was performed on three other cone-specific phototransduction genes: cyclic nucleotide-gated channel beta-3 (*Cngb3*), cyclic nucleotide phosphodiesterase 6c (*Pde6c*), and arrestin 3 (*Arr3*; Fig. 5E–G). An increase in the levels of all three mRNAs was detected in $Rds^{+/-}/Nrl^{-/-}$ eyes compared with $Rds^{-/-}/Nrl^{-/-}$ eyes. Specifically, *Cngb3* was 1.8-fold higher, *Pde6c* was 1.7-fold higher, and *Arr3* was 1.5-fold higher. Furthermore, the mRNA levels of *Cngb3* and *Pde6c* were increased in $Rds^{+/-}/Nrl^{-/-}$ eyes by 2.9-fold and 1.9-fold, respectively, compared with $Nrl^{-/-}$ eyes, which was similar to what was observed for *Gnat2* mRNA levels. Thus, the levels of Rds protein are temporally related to changes in mRNA and protein abundance of molecules required for phototransduction, in a manner that is linked to outer segment lamellae formation. Because all qRT-PCR data were normalized to levels of *Hprt*, and immunoblot densities were normalized to β-actin, these changes appear to be related to outer segment formation, rather than to changes in the relative number of viable photoreceptor cells.

In addition to the formation of cone outer segments lacking lamellae, we had previously observed that the formation of rosettes was greatly reduced in the $Rds^{-/-}/Nrl^{-/-}$ retina compared with the $Nrl^{-/-}$ retina (Farjo et al., 2006). To examine the molecular basis of this phenomenon, we conducted microarray analyses on WT, $Nrl^{-/-}$, $Rds^{-/-}$, and $Rds^{-/-}/Nrl^{-/-}$ retinas at P21. These analyses revealed increased expression of glial fibrillary acidic protein (*Gfap*) in the $Rds^{-/-}/Nrl^{-/-}$ compared with the $Nrl^{-/-}$ retina, which was subsequently confirmed using qRT-PCR and immunoblot analysis (Supplementary Fig. 1). Because Gfap up-regulation in Müller cells can occur during gliosis as a response to stress (Lewis and Fisher, 2003), we examined the histological organization of Müller cells in the retinas of these different mouse lines in conjunction with immunohistochemistry, with an antibody to glutamine synthetase (GS), a signature "housekeeping" enzyme present in Müller cells (Moscona and Linser, 1983;Vardimon et al., 1993; Fig. 6A). In WT, $Nrl^{-/-}$, and $Rds^{+/-}/Nrl^{-/-}$retinas, the OLM was well-formed and intact; in contrast, the OLM in $Rds^{-/-}/Nrl^{-/-}$ retinas was disrupted, and the junctional network appeared to be somewhat loose (Fig. 6A–L). These observations may signify a true disruption in the OLM or some aberrant morphology of Müller cell microvilli due to the change in photoreceptor population. For comparison, we did a similar analysis of

the OLM in rhodopsin-null (*Rho*$^{-/-}$) mice, in which the rod photoreceptors contain an inner segment, but no outer segment, and found the OLM to be comparable to that in WT retinas (Fig. 6C,F). This suggests that the dysmorphic outer segments of cones in the *Rds*$^{-/-}$/*Nrl*$^{-/-}$ mouse retina somehow contribute to the perturbation of the OLM. Furthermore, the number of photoreceptor rosettes/undulations was quantified throughout an entire retinal section from several *Nrl*$^{-/-}$, *Rds*$^{-/-}$/*Nrl*$^{-/-}$, and *Rds*$^{+/-}$/*Nrl*$^{-/-}$ eyes (Fig. 6M). This revealed that, in both models where the OLM associations appear normal (*Nrl*$^{-/-}$ and *Rds*$^{+/-}$/*Nrl*$^{-/-}$), there were nearly equal numbers of such rosettes/undulations, those numbers being significantly higher than the number observed in the *Rds*$^{-/-}$/*Nrl*$^{-/-}$ retina ($P < 0.01$, one-way ANOVA, Bonferroni's multiple-comparisons test). These findings suggest that an intact OLM and/or changes in Müller cell microvilli contribute to the formation of rosettes in the ONL of these retinas.

Finally, we had previously reported that the distended outer segments of the *Rds*$^{-/-}$/*Nrl*$^{-/-}$ were unable to associate properly with the cone matrix sheath (CMS; Farjo et al., 2006). Because one allele of Rds produced cone outer segments with lamellae, albeit oversized and disorganized, we hypothesized that this alteration may support CMS formation or association with the outer segment, similar to the support of OLM integrity. CMS localization and organization were examined in WT, *Nrl*$^{-/-}$, *Rds*$^{-/-}$, *Rds*$^{-/-}$/*Nrl*$^{-/-}$, and *Rds*$^{+/-}$/*Nrl*$^{-/-}$ retinas, using fluorescently tagged peanut agglutinin (PNA) to stain the CMS selectively (Johnson et al., 1986;Fig. 7). Similar to what was previously reported for the *Rds*$^{-/-}$/*Nrl*$^{-/-}$ retina (Farjo et al., 2006), the disorganized cone outer segments of the *Rds*$^{+/-}$/*Nrl*$^{-/-}$ retina (identified by their being labeled by anti-S-opsin) were not localized to the same histological layer as the PNA staining. Thus, the disruption of CMS interactions with the outer segment appears not to be a direct consequence of the presence or absence (relative abundance) of Rds but rather the result of improper outer segment structure.

DISCUSSION

Here, the phenotype of cone photoreceptor cells containing only one functional copy of Rds is presented. It is noteworthy that the data presented here are innately biased toward S-cones, because the photoreceptor population in the *Nrl*$^{-/-}$ retina is greatly enriched in S-cones and contains a complement of M-cones similar to that in the WT retina. In the complete absence of Rds, S-cones produce distended outer segment membranes that lack normal lamellar architecture but nonetheless are capable of limited amounts of phototransduction (Farjo et al., 2006). However, when one allele of Rds is present, cone photoreceptors form lamellae that are dysmorphic and longer than those in WT cone photoreceptors, being organized as membranous whorls, very similar to what has been observed in the rod photoreceptors of *Rds*$^{+/-}$ mice (Cheng et al., 1997;Nour et al., 2004). In terms of function, S-cones with only one copy of Rds provide better sensitivity to light stimuli than those completely lacking Rds; however, they are not as efficient as cones with a full complement of Rds protein. These results clearly demonstrate that one allele of Rds is not sufficient to promote proper outer segment lamellae formation in cones; however, lamellar morphogenesis is attempted, as is the case for disc morphogenesis in rods having only a single functional *Rds* allele (Hawkins et al., 1985). Furthermore, the outer segment structures observed in both *Rds*$^{-/-}$ and *Rds*$^{+/-}$ mice on the *Nrl*$^{-/-}$ background are consistent with the model of cone outer segment morphogenesis proposed by Eckmiller (1987,1990,1993), whereby cone lamellae formation consists of a sequential process of basal evagination of the photoreceptor ciliary plasma membrane, followed by a series of more distal invagination events at multiple points along the outer segment.

Our results also demonstrate that the relative abundance of Rds protein has consequences on the levels of cone-specific phototransduction-associated mRNAs and proteins. Although the mRNA levels of S-cone opsin were identical when comparing *Rds*$^{-/-}$/*Nrl*$^{-/-}$ and *Rds*$^{+/-}$/*Nrl*$^{-/-}$retinas, there was significantly more S-cone opsin protein present in the *Rds*$^{+/-}$/*Nrl*$^{-/-}$

retinas. This demonstrates that the synthesis and/or turnover of S-cone opsin protein are reliant on the presence of cone lamellae as a location for S-cone opsin protein deposition. These mice may serve as a useful model for understanding the precise mechanisms involved in regulating the steady-state levels of S-cone opsin protein within the cone. Furthermore, it was demonstrated that the mRNAs of several cone-specific phototransduction genes are concomitantly up-regulated when Rds protein is expressed, such as the mRNA and protein levels of Gnat2 in the presence of one Rds allele ($Rds^{+/-}/Nrl^{-/-}$ vs. $Rds^{-/-}/Nrl^{-/-}$). Based on these findings, there appear to be different mechanisms for regulating the amounts of S-cone phototransduction proteins in relation to the amount of outer segment lamellae. S-opsin showed steady mRNA levels but variations in protein levels as a consequence of the increased presence of outer segments, but other genes, such as Gnat2, Cngb3, and Pde6c, required changes in mRNA levels to produce subsequent changes in protein levels. Although Rds is commonly thought to be a structural protein, we hypothesize that it also may be involved in signaling pathways (yet to be elucidated) that regulate the levels of phototransduction genes in response to outer segment membrane formation. Rds is known to undergo light-dependent phosphorylation (Boesze-Battaglia et al., 1997), which may be a mechanism by which Rds exerts downstream effects on gene expression. Other membrane-associated molecules, such as integrins, initiate signaling pathways through their association with the extracellular matrix (Boulter and Van Obberghen-Schilling, 2006;Lo, 2006;Staunton et al., 2006). Insofar as the presence of Rds is required for proper localization of the CMS (Farjo et al., 2006), there could be undetermined interactions between Rds and the extracellular matrix that initiate signaling pathways. Alternatively, these mRNA increases could also just be an effect of enhanced stability of S-cone opsin protein and transcriptional changes required to support activation of S-opsin molecules. Future studies, using genomics to assess the complete effect of Rds abundance on the retinal transcriptome, may provide direct evidence regarding the specific signaling pathways that coordinate the changes in gene and protein expression observed here. Furthermore, it is of great interest to assess whether this phenomenon is reciprocated when a functional allele of other cone-specific phototransduction genes is eliminated.

By using histological and immunohistochemical methods, we discovered that OLM associations were perturbed in $Rds^{-/-}$ and $Rds^{-/-}/Nrl^{-/-}$ retinas but that this loss of OLM integrity was not observed when one functional *Rds* allele ($Rds^{+/-}/Nrl^{-/-}$) is present. There also seems to be a direct correlation between photoreceptor rosette formation (and outer nuclear layer undulations) and the integrity of the OLM, in that significantly fewer rosettes/undulations were present in $Rds^{+/-}/Nrl^{-/-}$ retinas. We propose, based on these data, that rosette formation is linked to OLM integrity or the interaction between photoreceptors and Müller cell microvilli. In retinas of $Nrl^{-/-}$mice, rosettes may develop as a consequence of the tensional forces exerted on cells by the OLM to keep the photoreceptor outer segments close to each other. The photoreceptor population lacks rods and is greatly enriched in S-cones in mice of this genotype, so the interphotoreceptor space lacks the structural support of rod outer segments that could balance these tensional forces and maintain proper lamination and alignment of the photoreceptor layer and support its normal apposition with the RPE. In contrast, the distended outer segments formed in the $Rds^{-/-}/Nrl^{-/-}$ retina cause a disruption in the OLM, which eases these tensions and reduces the number of rosettes/undulations. Such a disruption may be caused by RPE microvilli attempting to pinch off outer segment membranes from these aberrant cone outer segments, which lack normal lamellar structure. Furthermore, our observations could also be indicative of aberrant Müller cell morphology caused by the change in photoreceptor population. However, when lamellae formation is partially restored by the presence of one functional Rds allele (as in the $Rds^{+/-}/Nrl^{-/-}$ mouse retina); the OLM appears tight and intact, causing numbers of rosettes to form similar to the numbers observed in the $Nrl^{-/-}$ retina. In addition, even though one allele of Rds could support normal OLM integrity, it was insufficient to help coordinate the proper association between the CMS and the outer segment layer. Although this suggests that Rds is not directly tethering the outer segment to the CMS, that

possibility cannot be eliminated completely; it is possible that one allele of Rds is simply insufficient to generate the entire range of oligomeric complexes produced with two functional alleles.

Our examination of photopic ERG amplitudes in response to age in mice as a function of genotype demonstrated that $Nrl^{-/-}$ and $Rds^{+/-}/Nrl^{-/-}$ retinas lost their cone ERG amplitudes at approximately equal rates, which were significantly more accelerated than the rate of cone ERG loss in $Rds^{-/-}/Nrl^{-/-}$ mice. Although the photopic a-wave and b-wave amplitudes were initially higher in the genotypes containing Rds, all the values converged by 12 months of age (Fig. 4B). This trend suggests that cone photoreceptors devoid of Rds ($Rds^{-/-}/Nrl^{-/-}$) will maintain viability and function longer than those containing Rds ($Nrl^{-/-}$ and $Rds^{+/-}/Nrl^{-/-}$). These findings have potentially significant implications with regard to gene therapy approaches. Cone-specific silencing of Rds may be a reasonable therapeutic option for humans suffering from macular diseases resulting from Rds mutations. Further work using various gene transfer approaches in mouse mutants of Rds macular disease may provide additional evidence to help establish the practicality of such a treatment for cone-specific or cone-dominant retinal diseases.

Supplementary Material

Refer to Web version on PubMed Central for supplementary material.

Acknowledgements

The authors are grateful to Barbara A. Nagel, Didier Nuno, and Carla Hansens for technical contributions; to Drs. Cheryl Craft and Xuemei Zhu for generously supplying the Gnat1 and S-opsin antibodies used in this study; and to Dr. Robert Molday for generously supplying the rhodpsin 1D4 antibody. M.I.N. is the recipient of a Research to Prevent Blindness James S. Adams Scholar Award. S.J.F. is the recipient of a Research to Prevent Blindness Senior Scientific Investigator Award.

Grant sponsor: National Institutes of Health; Grant number: EY10609 (to M.I.N.); Grant number: EY007361 (to S.J.F.); Grant number: Core Grant for Vision Research EY12190 (to M.I.N.); Grant sponsor: Foundation Fighting Blindness (to M.I.N.); Grant sponsor: Norman J. Stupp Foundation Charitable Trust (to S.J.F.); Grant sponsor: Research to Prevent Blindness (to S.J.F.). Rafal Farjo's current address is Charlesson LLC, 800 Research Parkway, Suite 360, Oklahoma City, OK 73104.

LITERATURE CITED

Arikawa K, Molday LL, Molday RS, Williams DS. Localization of peripherin/rds in the disk membranes of cone and rod photoreceptors: relationship to disk membrane morphogenesis and retinal degeneration. J Cell Biol 1992;116:659–667. [PubMed: 1730772]

Boesze-Battaglia K, Goldberg AF. Photoreceptor renewal: a role for peripherin/rds. Int Rev Cytol 2002;217:183–225. [PubMed: 12019563]

Boesze-Battaglia K, Kong F, Lamba OP, Stefano FP, Williams DS. Purification and light-dependent phosphorylation of a candidate fusion protein, the photoreceptor cell peripherin/rds. Biochemistry 1997;36:6835–6846. [PubMed: 9184167]

Boulter E, Van Obberghen-Schilling E. Integrin-linked kinase and its partners: a modular platform regulating cell-matrix adhesion dynamics and cytoskeletal organization. Eur J Cell Biol 2006;85:255–263. [PubMed: 16546570]

Cheng T, Peachey NS, Li S, Goto Y, Cao Y, Naash MI. The effect of peripherin/rds haploinsufficiency on rod and cone photoreceptors. J Neurosci 1997;17:8118–8128. [PubMed: 9334387]

Damek-Poprawa M, Krouse J, Gretzula C, Boesze-Battaglia K. A novel tetraspanin fusion protein, peripherin-2, requires a region upstream of the fusion domain for activity. J Biol Chem 2005;280:9217–9224. [PubMed: 15591062]

Daniele LL, Lillo C, Lyubarsky AL, Nikonov SS, Philp N, Mears AJ, Swaroop A, Williams DS, Pugh EN Jr. Cone-like morphological, molecular, and electrophysiological features of the photoreceptors of the *Nrl* knockout mouse. Invest Ophthalmol Vis Sci 2005;46:2156–2167. [PubMed: 15914637]

Ding XQ, Stricker HM, Naash MI. Role of the second intradiscal loop of peripherin/rds in homo and hetero associations. Biochemistry 2005;44:4897–4904. [PubMed: 15779916]

Eckmiller MS. Cone outer segment morphogenesis: taper change and distal invaginations. J Cell Biol 1987;105:2267–2277. [PubMed: 3680382]

Eckmiller MS. Distal invaginations and the renewal of cone outer segments in anuran and monkey retinas. Cell Tissue Res 1990;260:19–28. [PubMed: 2340582]

Eckmiller MS. Shifting distribution of autoradiographic label in cone outer segments and its implications for renewal. J Hirnforsch 1993;34:179–191. [PubMed: 8228180]

Farjo R, Naash MI. The role of rds in outer segment morphogenesis and human retinal disease. Ophthalmic Genet 2006;27:117–122. [PubMed: 17148038]

Farjo R, Skaggs JS, Nagel BA, Quiambao AB, Nash ZA, Fliesler SJ, Naash MI. Retention of function without normal disc morphogenesis occurs in cone but not rod photoreceptors. J Cell Biol 2006;173:59–68. [PubMed: 16585269]

Goldberg AF. Role of peripherin/rds in vertebrate photoreceptor architecture and inherited retinal degenerations. Int Rev Cytol 2006;253:131–175. [PubMed: 17098056]

Hawkins RK, Jansen HG, Sanyal S. Development and degeneration of retina in rds mutant mice: photoreceptor abnormalities in the heterozygotes. Exp Eye Res 1985;41:701–720. [PubMed: 3830736]

Jansen HG, Sanyal S, De Grip WJ, Schalken JJ. Development and degeneration of retina in rds mutant mice: ultraimmunohistochemical localization of opsin. Exp Eye Res 1987;44:347–361. [PubMed: 2954840]

Johnson LV, Hageman GS, Blanks JC. Interphotoreceptor matrix domains ensheath vertebrate cone photoreceptor cells. Invest Ophthalmol Vis Sci 1986;27:129–135. [PubMed: 3080382]

Lewis GP, Fisher SK. Up-regulation of glial fibrillary acidic protein in response to retinal injury: its potential role in glial remodeling and a comparison to vimentin expression. Int Rev Cytol 2003;230:263–290. [PubMed: 14692684]

Lo SH. Focal adhesions: what's new inside. Dev Biol 2006;294:280–291. [PubMed: 16650401]

Mears AJ, Kondo M, Swain PK, Takada Y, Bush RA, Saunders TL, Sieving PA, Swaroop A. *Nrl* is required for rod photoreceptor development. Nat Genet 2001;29:447–452. [PubMed: 11694879]

Molday RS, MacKenzie D. Monoclonal antibodies to rhodopsin: characterization, cross-reactivity, and application as structural probes. Biochemistry 1983;22:653–660. [PubMed: 6188482]

Moscona AA, Linser P. Developmental and experimental changes in retinal glia cells: cell interactions and control of phenotype expression and stability. Curr Top Dev Biol 1983;18:155–188. [PubMed: 6132779]

Nikonov SS, Daniele LL, Zhu X, Craft CM, Swaroop A, Pugh EN Jr. Photoreceptors of $Nrl^{-/-}$ mice coexpress functional S- and M-cone opsins having distinct inactivation mechanisms. J Gen Physiol 2005;125:287–304. [PubMed: 15738050]

Nir I, Papermaster DS. Immunocytochemical localization of opsin in the inner segment and ciliary plasma membrane of photoreceptors in retinas of rds mutant mice. Invest Ophthalmol Vis Sci 1986;27:836–840. [PubMed: 2939037]

Nour M, Ding XQ, Stricker H, Fliesler SJ, Naash MI. Modulating expression of peripherin/rds in transgenic mice: critical levels and the effect of overexpression. Invest Ophthalmol Vis Sci 2004;45:2514–2521. [PubMed: 15277471]

Ritter LM, Boesze-Battaglia K, Tam BM, Moritz OL, Khattree N, Chen SC, Goldberg AF. Uncoupling of photoreceptor peripherin/rds fusogenic activity from biosynthesis, subunit assembly, and targeting: a potential mechanism for pathogenic effects. J Biol Chem 2004;279:39958–39967. [PubMed: 15252042]

Sanyal S, Jansen HG. Absence of receptor outer segments in the retina of rds mutant mice. Neurosci Lett 1981;21:23–26. [PubMed: 7207866]

Sanyal S, Zeilmaker GH. Development and degeneration of retina in rds mutant mice: light and electron microscopic observations in experimental chimaeras. Exp Eye Res 1984;39:231–246. [PubMed: 6489472]

Sanyal S, Dees C, Zeilmaker GH. Development and degeneration of retina in rds mutant mice: observations in chimaeras of heterozygous mutant and normal genotype. J Embryol Exp Morphol 1986;98:111–121. [PubMed: 3655642]

Staunton DE, Lupher ML, Liddington R, Gallatin WM. Targeting integrin structure and function in disease. Adv Immunol 2006;91:111–157. [PubMed: 16938539]

Steinberg RH, Fisher SK, Anderson DH. Disc morphogenesis in vertebrate photoreceptors. J Comp Neurol 1980;190:501–508. [PubMed: 6771304]

Vardimon L, Ben-Dror I, Havazelet N, Fox LE. Molecular control of glutamine synthetase expression in the developing retina tissue. Dev Dyn 1993;196:276–282. [PubMed: 8106020]

Yoshida S, Mears AJ, Friedman JS, Carter T, He S, Oh E, Jing Y, Farjo R, Fleury G, Barlow C, Hero AO, Swaroop A. Expression profiling of the developing and mature *Nrl*$^{-/-}$ mouse retina: identification of retinal disease candidates and transcriptional regulatory targets of *Nrl*. Hum Mol Genet 2004;13:1487–1503. [PubMed: 15163632]

Yu J, He S, Friedman JS, Akimoto M, Ghosh D, Mears AJ, Hicks D, Swaroop A. Altered expression of genes of the Bmp/Smad and Wnt/calcium signaling pathways in the cone-only *Nrl*$^{-/-}$ mouse retina, revealed by gene profiling using custom cDNA microarrays. J Biol Chem 2004;279:42211–42220. [PubMed: 15292180]

Zhu X, Brown B, Li A, Mears AJ, Swaroop A, Craft CM. GRK1-dependent phosphorylation of S and M opsins and their binding to cone arrestin during cone phototransduction in the mouse retina. J Neurosci 2003;23:6152–6160. [PubMed: 12853434]

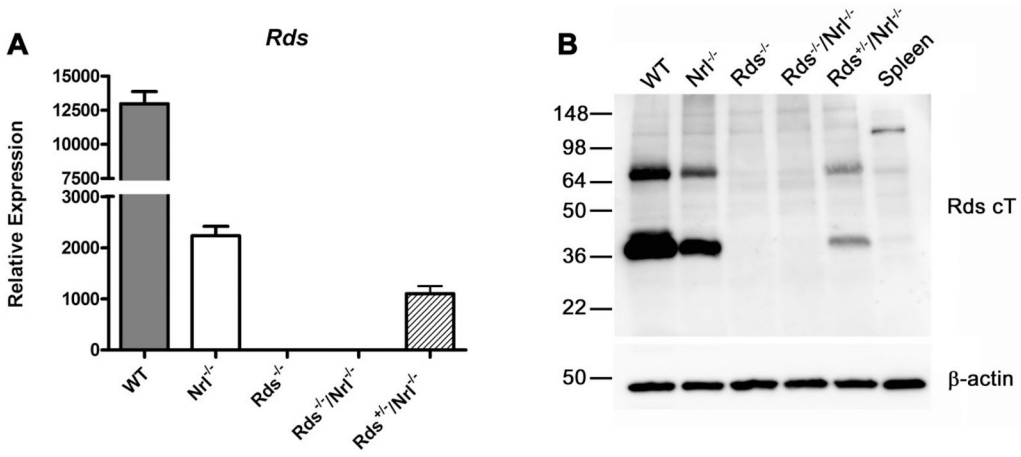

Fig 1.

Levels of Rds mRNA and protein in *Rds*$^{+/-}$/*Nrl*$^{-/-}$ eyes. **A:** qRT-PCR analysis of mouse eyes (mean ± SD, N = 3), normalized relative to *Hprt*. **B:** Correlative Western blot analysis, demonstrating the relative abundance of Rds protein as a function of genotype. Note the presence of an immunopositive band at M_r ~75–80 kDa, indicating that expression of one allele of Rds is sufficient to promote Rds dimer formation.

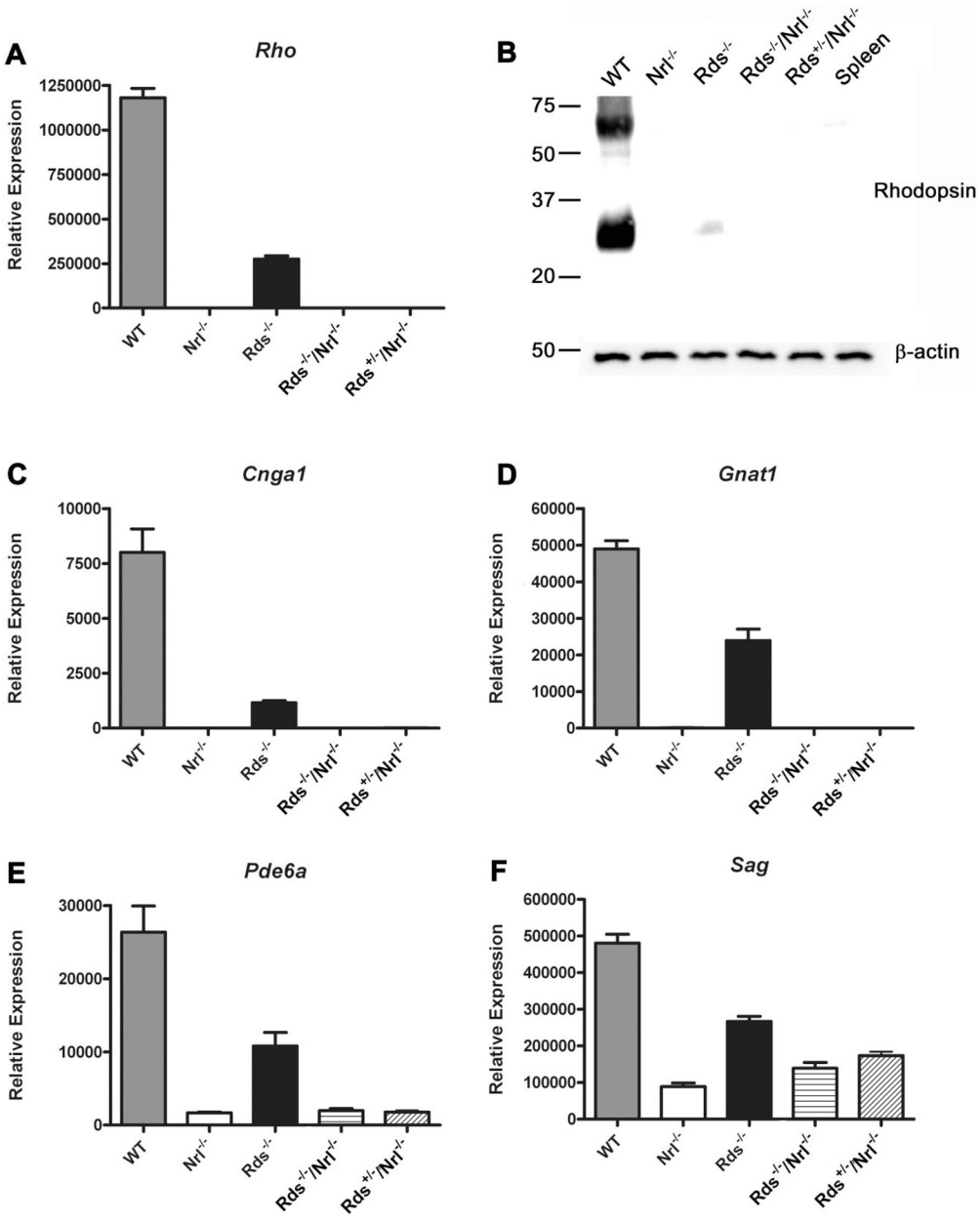

Fig 2.

Expression levels of phototransduction genes in different models at P30. **A:** qRT-PCR analysis (mean ± SD, N = 3), normalized to *Hprt*, demonstrating the absence of rhodopsin (*Rho*) mRNA expression in all genotypes having the *Nrl*$^{-/-}$ background. **B:** Correlative Western blot probed with antirhodopsin antibodies. Note that, except in WT and (minimally) in Rds$^{-/-}$ retinas, rhodopsin is absent. **C–F:** qRT-PCR analysis of photoreceptor-specific genes (mean ± SD, N = 3), normalized to *Hprt. Cnga1*, cyclic nucleotide-gated channel alpha-1; *Gnat1*, rod transducin; *Pde6a*, cyclic nucleotide phosphodiesterase 6a; *Sag*, S-antigen.

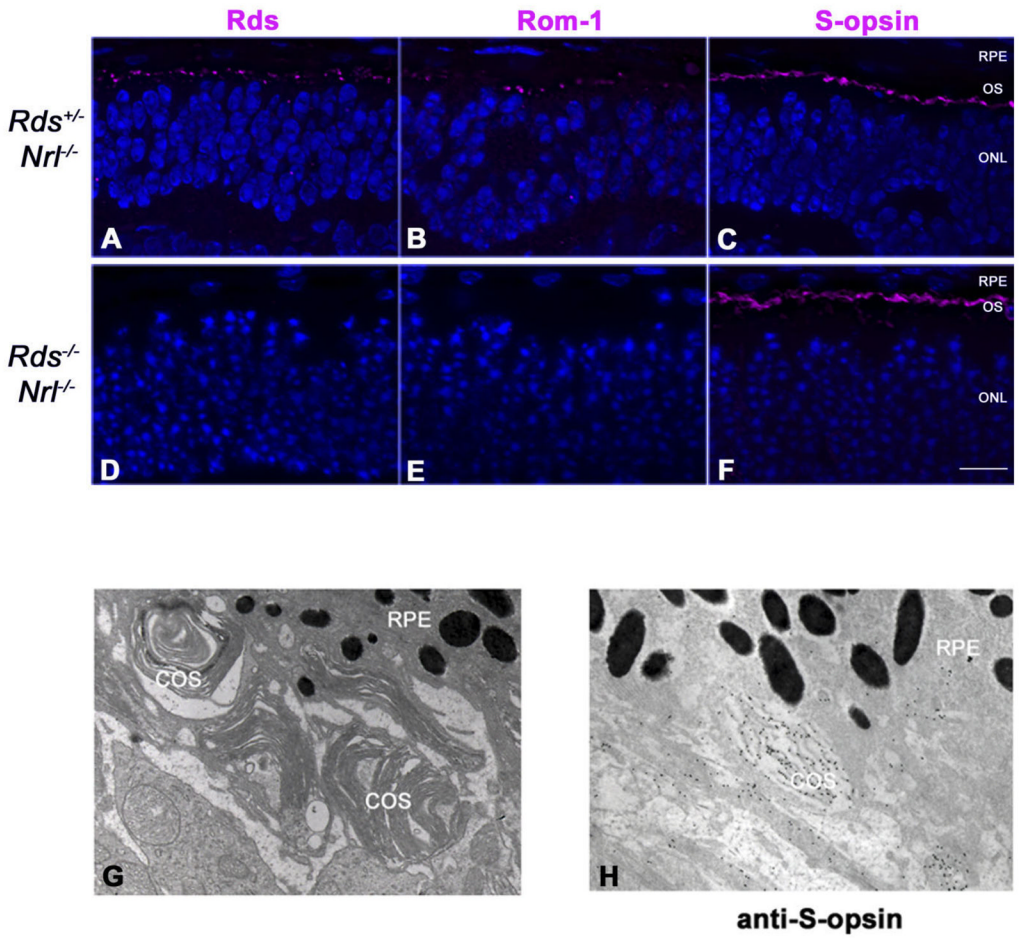

Fig 3.

Immunolocalization of outer segment proteins and analysis of outer segment ultrastructure as a function of Rds expression on the $Nrl^{-/-}$ background. **A–F:** Paraffin sections of P30 mouse eyes were immunostained with antibodies against Rds, Rom-1, and S-opsin, plus Alexa-555-conjugated secondary antibodies (red), counterstained with DAPI (blue) to visual nuclei, and examined by confocal fluorescence microscopy. Note the punctuate labeling pattern of Rds and Rom-1 in the $Rds^{+/-}$ retina, and the complete absence of such labeling in the $Rds^{-/-}$ retinas. Anti-S-cone opsin labeled structures in the outer photoreceptor layer in retinas of both genotypes; however, there are focal regions in the $Rds^{+/-}/Nrl^{-/-}$ retina that appear more intensely labeled. **G:** Transmission electron microscopy demonstrating the retinal ultra-structure of P30 $Rds^{+/-}/Nrl^{-/-}$ mice. Membranous whorls and elongated lamellae make up a majority of the outer segment structures, which contain S-cone opsin, as revealed by immunogold labeling (**H**). Scale bar = 10 μm in F (applies to A–F).

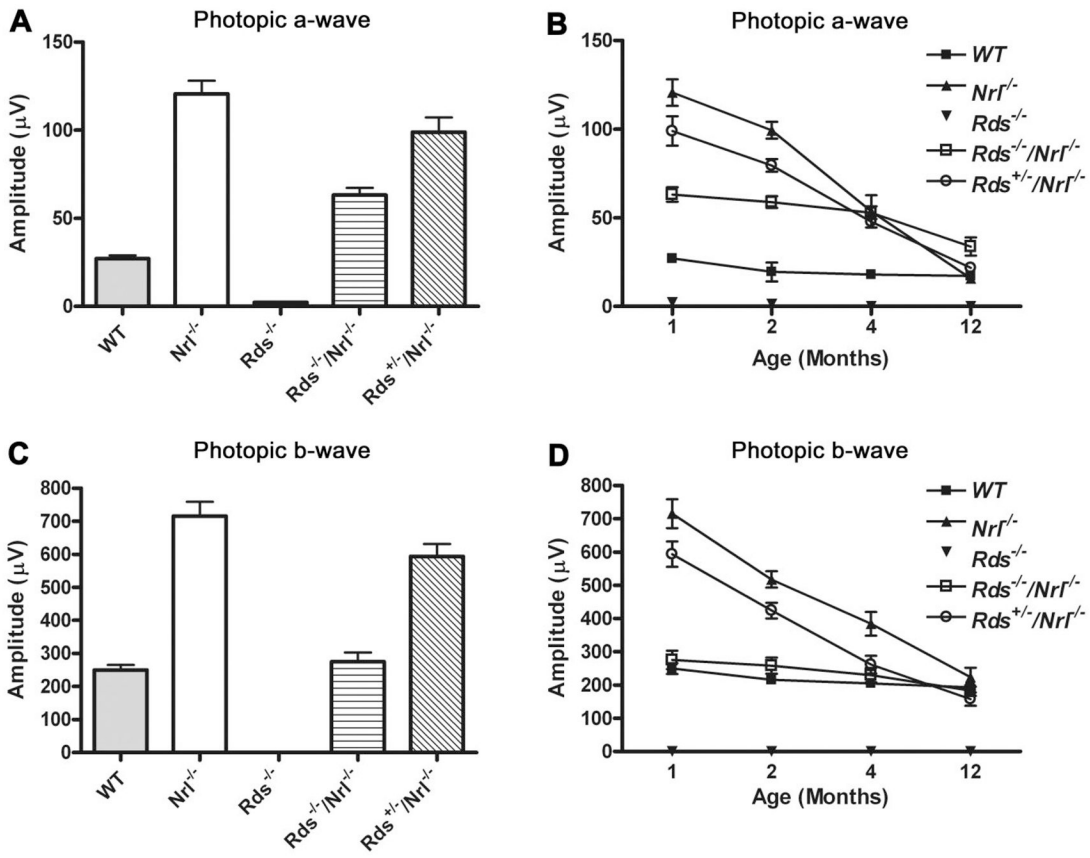

Fig 4.

Functional analysis of the different models. **A,C:** Photopic a-wave and b-wave amplitudes (mean ± SD, N = 3) of WT, $Nrl^{-/-}$, $Rds^{-/-}$, $Rds^{-/-}/Nrl^{-/-}$, and $Rds^{+/-}/Nrl^{-/-}$ mice at P30. Note that amplitudes of $Rds^{+/-}/Nrl^{-/-}$ retinas are about twofold higher than those of $Rds^{-/-}/Nrl^{-/-}$ retinas, but ~17% less than those of $Nrl^{-/-}$ retinas. **B,D:** Loss of photopic a-wave and b-wave amplitude as a function of postnatal age.

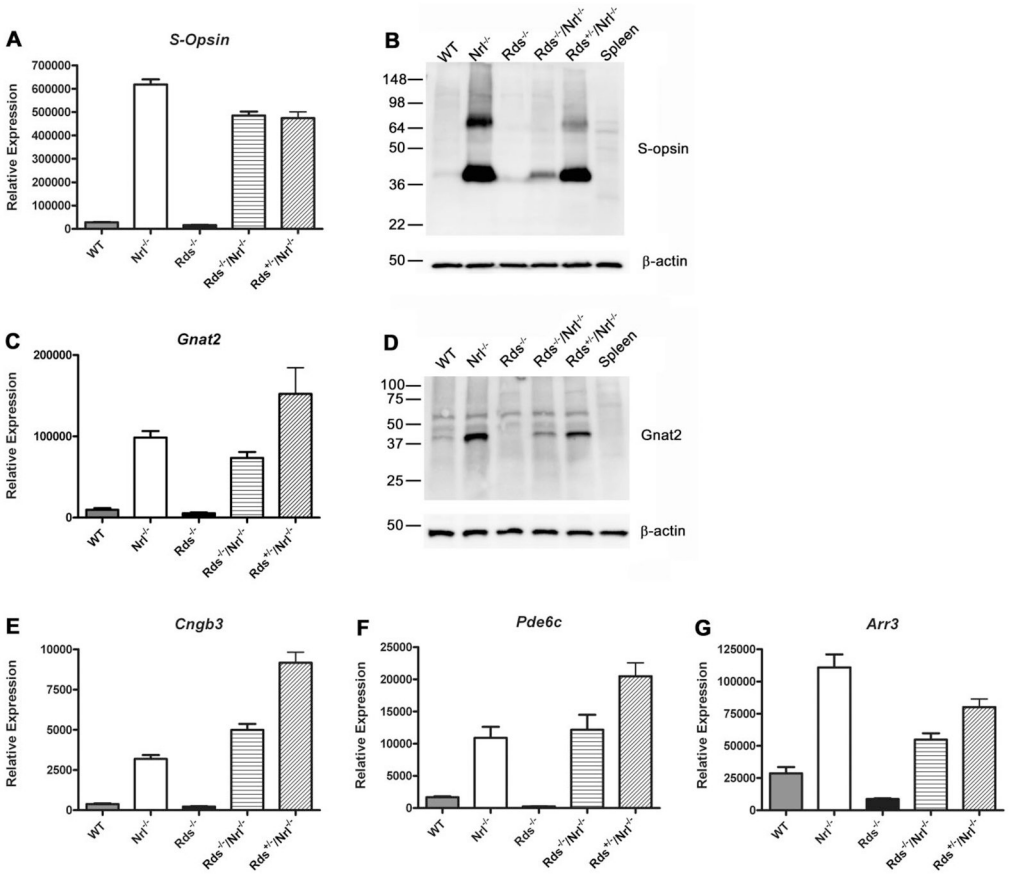

Fig 5.

Expression levels of cone phototransduction genes in the different models at P30. **A:** qRT-PCR analysis of S-opsin mRNA levels (mean ± SD, N = 3), normalized to *Hprt*. Note the elevation of S-opsin mRNA levels in all $Nrl^{-/-}$ genotypes and that expression of one allele of Rds has no effect on S-opsin mRNA levels. **B:** Correlative Western blot analysis of retinas, probed with anti-S-cone opsin. **C:** qRT-PCR analysis of *Gnat2* mRNA levels (mean ± SD, N = 3), normalized to *Hprt*. Note the elevated *Gnat2* mRNA levels in $Rds^{+/-}/Nrl^{-/-}$ eyes compared with eyes from $Rds^{-/-}/Nrl^{-/-}$ and $Nrl^{-/-}$ mice. **D:** Correlative Western blot analysis of retinas, probed with anti-Gnat2. **E–G:** qRT-PCR analysis of additional photoreceptor-specific mRNAs, normalized to *Hprt* (means ± SD, N = 3). Cyclic nucleotide-gated channel beta-3 (*Cngb3*), transducin (*Gnat2*), cyclic nucleotide phosphodiesterase 6c (*Pde6c*), and arrestin-3 (*Arr3*).

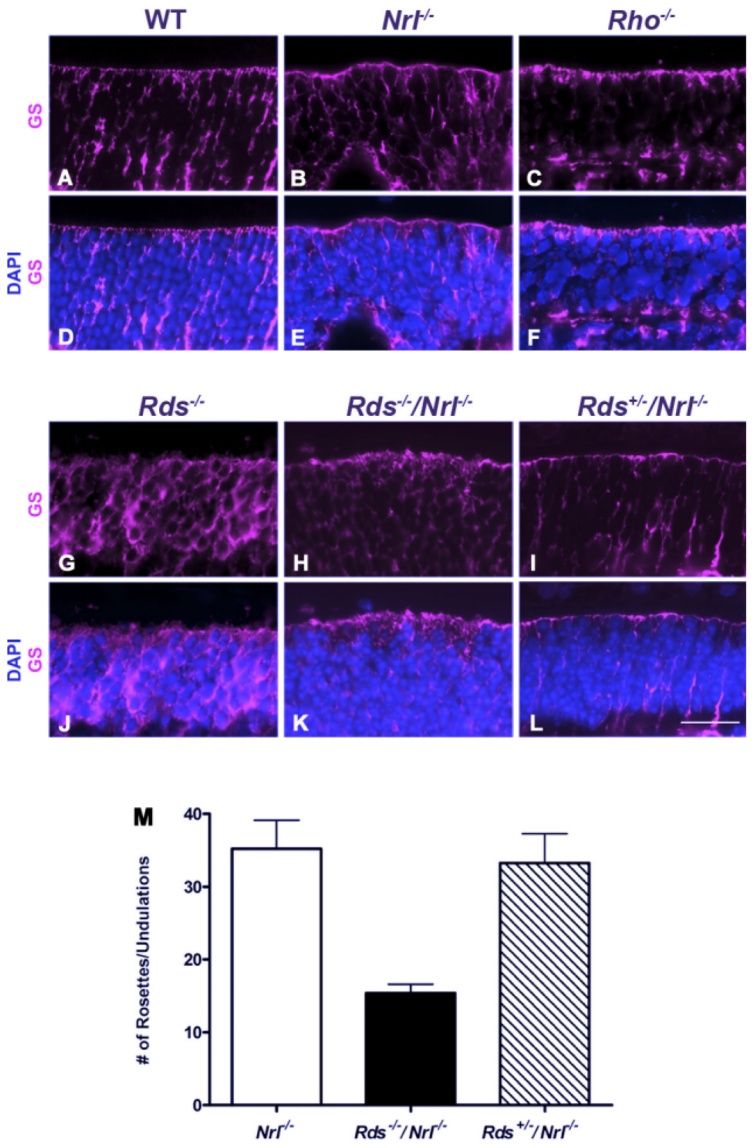

Fig 6.

Müller cell morphology, glutamine synthetase distribution, and photoreceptor rosette/undulation quantification in the different models. **A–L:** Retinal sections from WT, *Nrl*$^{-/-}$, *Rds*$^{-/-}$, Rho$^{-/-}$, *Rds*$^{-/-}$/*Nrl*$^{-/-}$, and *Rds*$^{+/-}$/*Nrl*$^{-/-}$ at P30 were labeled with antibodies to glutamine synthetase (GS) and Alexa-555-conjugated secondary antibodies (red) to visualize Müller cells and their processes, counterstained with DAPI (blue) to visual ONL nuclei, and examined by confocal fluorescence microscopy. **M:** Quantification of photoreceptor rosettes and ONL undulations across the entire expanse of retinal sections from *Nrl*$^{-/-}$, *Rds*$^{-/-}$/*Nrl*$^{-/-}$, and *Rds*$^{+/-}$/*Nrl*$^{-/-}$ eyes (mean ± SD, N = 4 each). Scale bar = 10 μm.

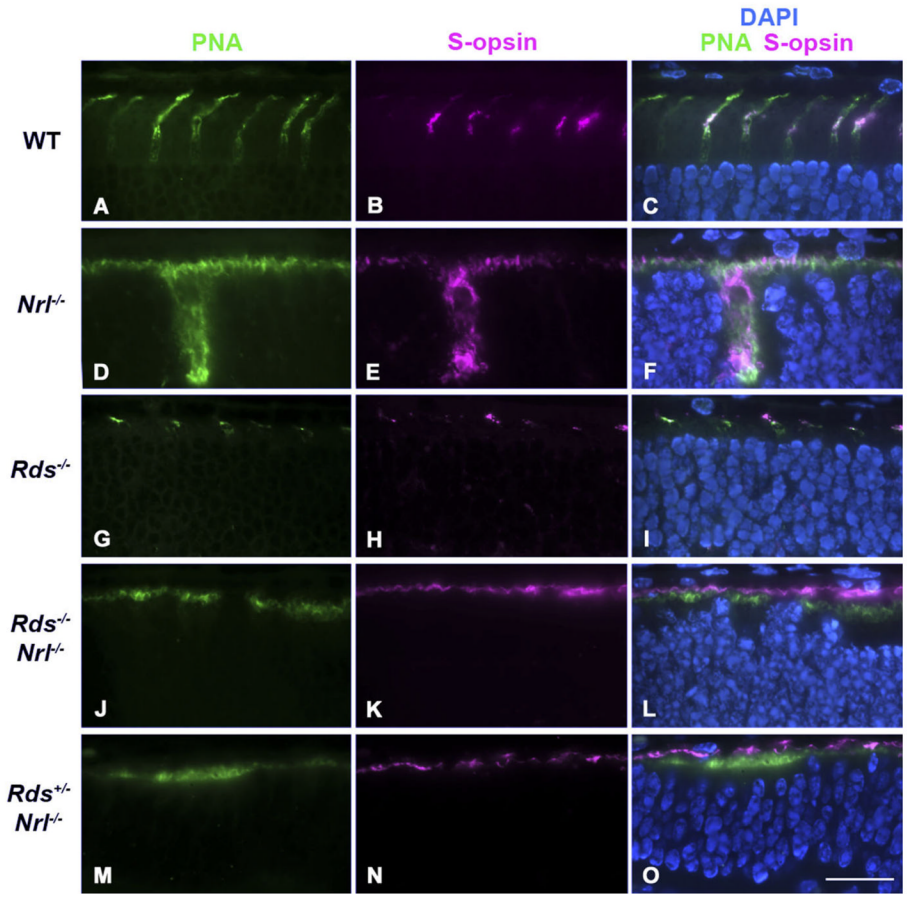

Fig 7.

Interaction between cone outer segments and CMS as a function of genotype. **A–O:** Immunohistochemistry was performed with anti-S-cone opsin and Alexa-555-conjugated secondary antibodies (red) to visualize cone outer segments and Alexa-488-conjugated PNA (green) to visualize the CMS in retinal sections from WT, $Nrl^{-/-}$, $Rds^{-/-}$, $Rds^{-/-}/Nrl^{-/-}$, and $Rds^{+/-}/Nrl^{-/-}$ eyes at P30. Sections were counterstained with DAPI (blue) to visual nuclei, then examined by confocal fluorescence microscopy. Coincidence of outer segments and CMS is denoted by orange fluorescence. Scale bar = 10 μm.